HANSER

Sample Pages

Polymer Testing

Translated by Paul I. Anderson

Herausgegeben von Wolfgang Grellmann, Sabine Seidler

ISBN (Buch): 978-1-56990-548-7

ISBN (E-Book): 978-1-56990-549-4

For further information and order see

http://www.hanser-fachbuch.de/978-1-56990-548-7

or contact your bookseller.

Table 4.4: Compressive strength of selected polymers [1.48]

Material	σ_M (MPa)	Material	σ_M (MPa)
Thermosets		*Thermoplastics unreinforced*	
Phenole resin	170	PMMA	110
Urea resin	200	PTFE	12
Melamine–formaldehyde resin	200	*Thermoplastics reinforced*	
UP resin	150	PP + 30 wt.-% GF	60
EP resin	150	PA 6 + 30 wt.-% GF	160
PUR	110	PA 66 + 30 wt.-% GF	170

4.3.5 Bend Tests on Polymers

4.3.5.1 Theoretical Basis of the Bend Test

Flexural loading is one of the most common types of load encountered in practice. Thus it is highly significant for determining characteristic values of polymers and fiber composite materials. This type of load is used in the following test procedures:

- Bend test for characterizing thermoplastic and thermosetting molding compounds and filled as well as reinforced composite materials,
- Mechanical-thermal flexural loading for measuring heat-distortion resistance in the HDT test, as well as
- Mechanical-environmental flexural loading for measuring environmental stress cracking resistance.

The quasi-static bend test is used especially for testing brittle materials whose failure behavior causes technical problems with tensile tests. For polymers, this test is used on the following materials according to the specifications of test standards:

- Thermoplastic injection and extrusion molding compounds, including filled and reinforced molding compounds, as well as rigid thermoplastic sheets,
- Thermosetting molding compounds, including filled and reinforced composite materials,
- Thermosetting sheets, including laminates,
- Fiber-reinforced thermosetting and thermoplastic composite materials containing both unidirectional and non-unidirectional reinforcements, and
- Thermotropic liquid-crystalline polymers.

However, this test method is not suited for rigid foams or sandwich structures with foam cores.

Under flexural load, as under tensile or compression load, the various deformation components have to be considered that are dependent on time and load. Depending on the type of polymer, linear-elastic, linear-viscoelastic, non-linear viscoelastic and plastic deformation components also occur. The ratio of deformation components to total deformation depends on the particular polymer as well as on loading conditions (temperature and test speed). Therefore, the value acquired in the bend test is a function of deformation, strain rate, load or stress, temperature and the internal state of the specimen. In actual testing practice, three-point and four-point bend test equipment is available for performing bend tests (Fig. 4.41). In view of the occurring loads, the four-point bend test is the fundamentally more suitable method due to the constant bending moment and the freedom from transverse force.

With this arrangement, no corrective measures are required in the case of off-center fracture of the specimen. Its disadvantages are its technically more complicated construction and work-intensive handling; in addition, it requires an extremely precise deflection measuring device. For these reasons in particular, the three-point bend test is specified in ISO 178 as the test method for plastics, even though the four-point bend test produces more precise and reproducible results. Due to structural deficiencies in specimens, eccentric fracture can occur under three-point bend loading; as long as fracture occurs in the median third of the specimen that is acceptable for value acquisition.

The same fundamental requirements hold for performing bend tests as for tensile and compression tests (see also Section 4.3.2.1), i.e., load must be applied without impact and increase steadily. A uniaxial normal stress state should arise in the specimen, whereby influences from test equipment, shearing by transverse force, as well as compression at the supports, have to be negligible. The specimen must also be free of geometric imperfections, such as notches, and its cross-section must remain plane during the test, i.e., no warping is to occur.

With these requirements and the general differential equation of the elastic bending line (Eq. 4.122), the relation between deflection, E modulus and specimen geometry can be derived for the case of three-point bending (Fig. 4.42).

$$\frac{f''(x)}{\left[1+f'^{2}(x)\right]^{3/2}} = -\frac{M_b(x)}{EI} \tag{4.122}$$

In this equation, $M_b(x)$ is local variable bending moment, EI flexural stiffness and df/dx the slope of the bending line. Since this differential equation of the deformed cantilever beam can only be solved numerically, and is thus difficult to handle, the simplified Eq. 4.123 is used in actual practice, being valid for small deflections f and

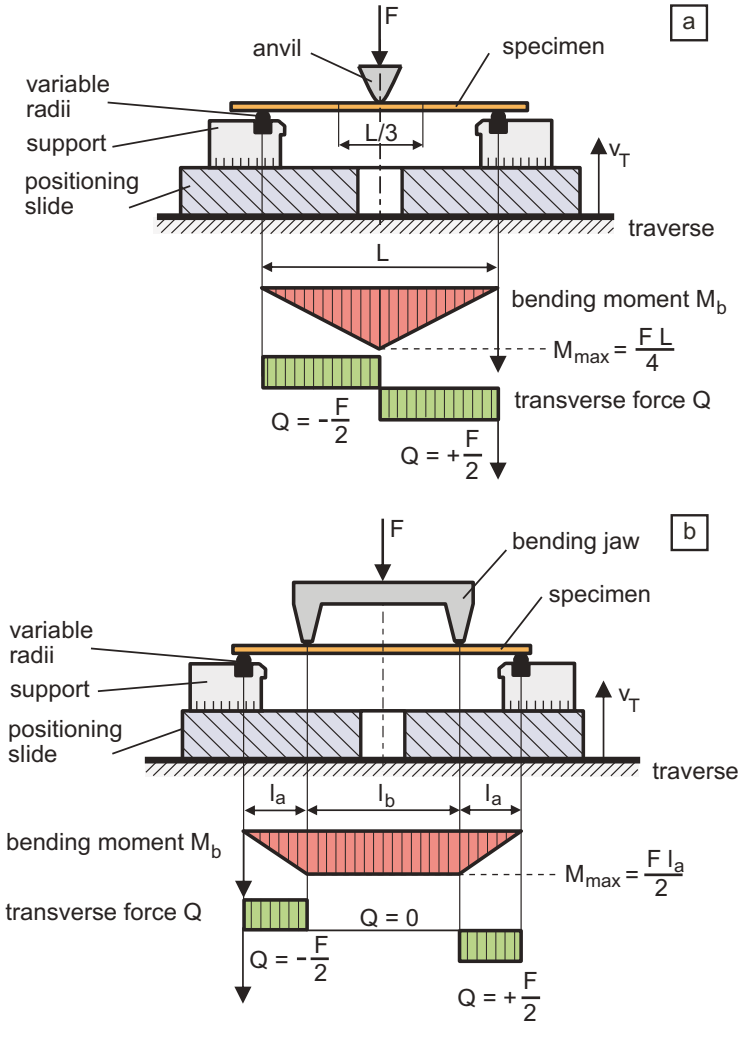

Fig. 4.41: Construction diagram of three- (a) and four-point bend test equipment (b)

slope $df/dx \approx 0$ [4.60].

$$f''(x) = -\frac{M_b(x)}{EI} \tag{4.123}$$

The elastic bending line for three-point bending, taking boundary conditions into consideration, yields the following:

$$f(x) = \frac{1}{EI}\left(\frac{F}{16}L^2x - \frac{F}{12}x^3\right) \tag{4.124}$$

For technical measurement purposes, the middle deflection f at point $x = L/2$ is especially interesting:

$$f = \frac{F\,L^3}{48\,E\,I} \tag{4.125}$$

Assuming linear-elastic material behavior, strain and stress are distributed symmetrically over the cross-section (Fig. 4.42b), whereby an unstressed and unstrained fiber, also called a neutral fiber, appears in the center of the specimen. Since external stress is distributed linearly over the cross-section, the highest tensile or compression stress always occurs in the peripheral fibers of the bend specimen, whereby the sign is generally ignored in actual practice (Eq. 4.126).

$$\sigma_f = \frac{M_b}{I}\frac{h}{2} \tag{4.126}$$

Using the maximum bending moment in the specimen center $M_b = FL/4$ and the axial moment of inertia in prismatic specimen I (Eq. 4.127), we obtain the equation for calculating flexural stress σ_f in the three-point bend test (Eq. 4.128).

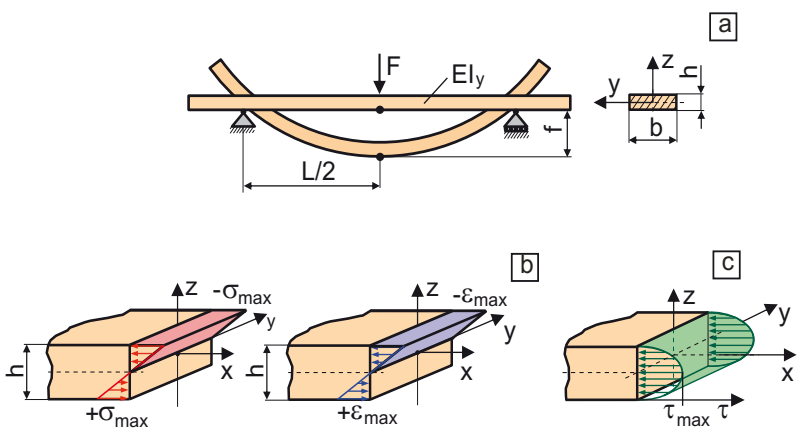

Fig. 4.42: Three-point bend specimen (a), distribution of normal stress and strain (b), as well as shear stress distribution (c) over specimen cross-section

$$I = \frac{b h^3}{12} \tag{4.127}$$

$$\sigma_f = \frac{3 F L}{2 b h^2} \tag{4.128}$$

This yields a load level varying over specimen height or thickness, whereby the individual deformation components can occur simultaneously in time and location.

When tensile and compression stress deformation behavior are identical, only singular, planar symmetrical layers in the specimen reach yield stress (tensile load) or compressive strain at yield (compression load). Thus the yield stress observed is never as pronounced as in the tensile test. When a yield point is reached, the effects on the actually developing stress and deformation region can be seen particularly in the peripheral fiber of the specimen, in contrast to theoretical compressive behavior. Due to these circumstances, a stress distribution over cross-section results that diverges from linearity, particularly when the yield point, i.e., beginning plastic deformation is reached. If there are significant differences of tensile and compressive behavior for the material investigated (Fig. 4.40), displacement of neutral fibers can occur, leading to asymmetrical stress distribution over the cross-section.

Using *Hooke's* law and maximum flexural stress σ_f in Eq. 4.128 we obtain the relationship between measured quantity f and dimensionless peripheral fiber strain ε_f:

$$\varepsilon_f = \frac{6 f h}{L^2} \tag{4.129}$$

In order to measure traverse path, i.e., to determine the deflection between bend anvil and supports (Fig. 4.42a), the elasticity modulus E_f is obtained as follows:

$$E_f = \frac{F L^3}{4 f b h^3} \tag{4.130}$$

The relationship between cross-head speed v_T and desired peripheral fiber strain rate $d\varepsilon_f/dt$ is important for setting the universal testing machine:

$$\dot{\varepsilon}_f = \frac{d\varepsilon_f}{dt} = \frac{6 v_T h}{L^2} \tag{4.131}$$

Besides normal stress, additional shear stress (Fig. 4.42c) develops in the specimen that can influence the result of the bend test. In order to minimize this effect, the ratio of support length L to specimen height h must be considered when testing plastics:

$$L = (16 \pm 1)\, h \tag{4.132}$$

For very thick specimens or materials containing coarse fillers, a relatively large *L/h* ratio may be required to avoid delaminations due to shearing. This is especially true for laminates or other layered plastics, except when testing for interlaminar shear strength (short-beam test). In this case, the ratio *L/h* should range from 20 to 25 to eliminate the shear stress portion. For very soft plastics, such as PE, the support span can be increased or the support radius altered in order to reduce the amount of indention caused by the supports on the specimen. If only very short specimens are available, deflection can also be determined by strain gauges instead of measuring traverse path (Fig. 4.43).

When measuring middle deflection using a deflection sensor (Fig. 4.43a), the measurement result does not include indenting into the specimen by the bend anvil, i.e., Eqs. 4.125 to 4.131 are still valid. If fork sensors such as in Fig. 4.43b are used, indenting by the supports is also eliminated; however, different equations have to be used to calculate deflection *f*, peripheral fiber strain and modulus E_f:

$$f = \frac{F L_G^2}{96 E I} (3L - L_G) \tag{4.133}$$

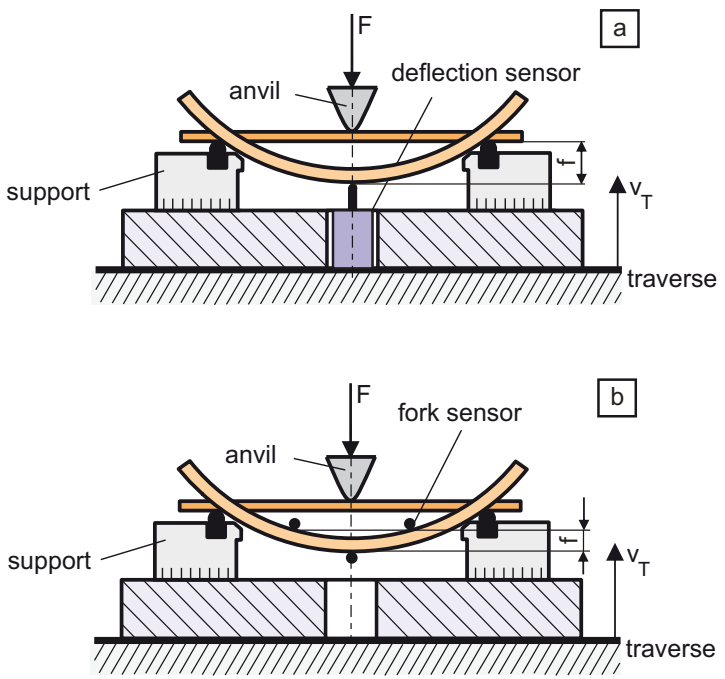

Fig. 4.43: Use of different strain measurement systems for determining deflection with a deflection sensor (a) and a fork sensor (b)

$$\varepsilon_f = \frac{12 f h L}{L_G^2 (3L - L_G)} \tag{4.134}$$

$$E_f = \frac{F L_G^2 (3L - L_G)}{8 f b h^3} \tag{4.135}$$

If the specimens are very thick or very short, support indentation can become a problem for the measurement technique. To eliminate the problem, larger support radii are used, which, if deflection is considerable, can cause specimen roll-off, resulting in a shortening of the support span and thus influencing the test result. In addition, normal stresses often are generated by friction, bringing about a displacement of neutral fiber and, thereby, stress distribution. More extensive information on numerical correction for such measurement effects is provided by [4.61] among others. When bend tests are being performed, care must be taken, as with other basic mechanical tests, to position the specimens as precisely in the load line as possible; otherwise bending can be skewed, or torsional moment can influence the measurement results. For this reason, no flexible, self-adjusting supports should be used. The forces occurring in actual testing practice are not sufficient to maintain plane position of the specimen. If the test equipment has centering devices, such as arresting stoppers on the supports, these should always be utilized.

By analogy with the tensile or compression test on plastics, pure bending is overlaid by relaxation and creep processes in the quasi-static bend test as well, as exhibited by the strong dependence of test results on test speed and temperature. Strict adherence to test conditions is indispensable to obtain comparable results.

4.3.5.2 The Standardized Bend Test

ISO 178 is used for performing bend tests on plastics. The specimen of preference exhibits dimensions of $80 \times 10 \times 4\ mm^3$ and can be produced directly by injection molding or by removing the shoulders from type 1A multipurpose specimens (Fig. 4.44a, Table 4.2). The latter procedure has the advantage of comparable orientation and residual stress state for evaluating material properties.

When specimens with different dimensions are used, Eq. 4.136 has to be fulfilled:

$$l = (20 \pm 1) h \tag{4.136}$$

With thermoplastic or thermosetting sheets or with textile and long-glass-fiber reinforced plastics, the specimen can be up to 80 mm wide and up to 50 mm thick; however, a correspondingly long specimen and wide supports have to be used. When testing anisotropic materials, such as laminates or laminated plastics, specimen types

(Fig. 4.44b) should be selected such that the main loading direction is used for acquiring values. If the differences in the various directions are considerable, tests are required on specimens with differing orientations, whereby collation of the measurement results with the orientation direction must be assured. For all types of specimens, it is essential that they not exhibit any kinking, edge rounding, scratches or fissures. Specimens with very sharp cooling contraction and shrink marks cannot be used.

Test speed in the bend test is generally set to correspond with the particular product standard; ISO 178 permits test speeds from 1 mm min^{-1} to 500 mm min^{-1}.

If there are no such specifications, according to the standard, the traverse speed v_T is selected so that it is close to the normal flexural strain rate of $d\varepsilon_f/dt = 1\ \%\ min^{-1}$. For preferred specimens with dimensions of $80 \times 10 \times 4\ mm^3$ and a support span $L = 64$ mm, this yields a cross-head speed of 2 mm min^{-1} (Eq. 4.131). With materials with pronounced initial behavior, a preload F_v can be used; however, the resulting strains must not exceed 0.05 % with reference to measurement of the E modulus. By analogy with the tensile and compression test, it is recommended that the test apparatus for bend tests be set up with a system prestress of 90 to 95 % nominal load and with rigid set-up specimens to avoid setting motion during the test. Elasticity modulus E_f under flexural loading is acquired under the same conditions as in tensile

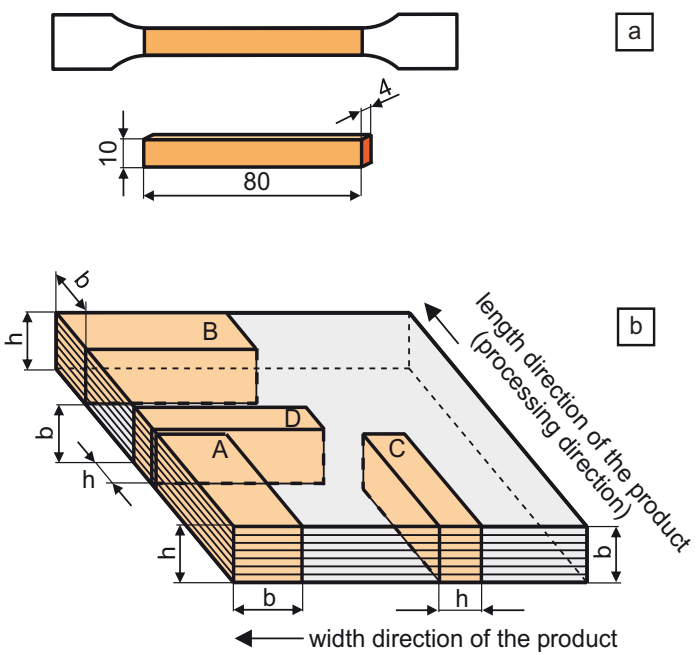

Fig. 4.44: Specimens for the bend test according to ISO 178

and compression tests, i.e., as a secant modulus (Fig. 4.27a) in a range of 0.05 to 0.25 % peripheral fiber strain (Eq. 4.136). The same test speed is used as in the bend test itself.

$$E_f = \frac{\sigma_{f2} - \sigma_{f1}}{\varepsilon_{f2} - \varepsilon_{f1}} = \frac{\Delta\sigma}{0.002} \tag{4.137}$$

Figure 4.45 shows typical flexural stress–peripheral fiber strain diagrams of various polymers. Diagram (a) in Fig. 4.45 shows the brittle fracture behavior of materials such as PS or PMMA.

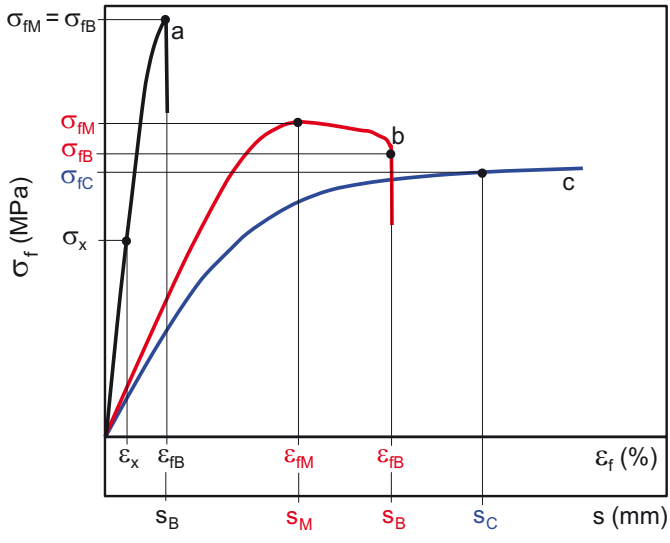

Fig. 4.45: Typical flexural stress–peripheral fiber strain diagrams of polymers in the bend test

When the material behavior is ductile (curve (b) in Fig. 4.45), the force reaches a peak and fracture occurs prior to reaching so-called conventional deflection s_C. In this case, flexural strength can be measured at maximum load. If neither a peak in force, nor fracture occurs prior to conventional deflection, flexural stress at conventional deflection σ_{fC} is determined at this position; this material behavior is still considered ductile. According to Fig. 4.45, the material parameters explained in the following can be determined for various plastic materials.

Flexural strength σ_{fM}: the maximum flexural stress tolerated by the specimen during the experiment. In the case of material behavior as shown in diagram (a) in Fig. 4.45, this value is identical to σ_{fB}.

$$\sigma_{fM} = \frac{3 F_{max} L}{2 b h^2} \tag{4.138}$$

Flexural stress at break σ_{fB}: this value is determined if specimen break occurs during the experiment. Of course, it depends to a high degree on the conditions set for the break detector threshold on the universal testing machine.

$$\sigma_{fB} = \frac{3 F_B L}{2 b h^2} \tag{4.139}$$

Flexural stress at conventional deflection σ_{fC}: this parameter is determined if the specimen fails to break, or if no peak force occurs. In this case, the flexural stress is calculated with the recorded conventional deflection $s_C = 1.5\ h$. Given a support span of $L = 16\ h$, this deflection value corresponds to a peripheral fiber strain ε_f of 3.5 %.

$$\sigma_{fC} = \frac{3 F_C L}{2 b h^2} \tag{4.140}$$

Flexural strain at flexural strength ε_{fM}: the peripheral fiber strain determined at the position of flexural strength. This value can be stated dimensionless or as a percentile. The value can be identical with flexural strain at break if the material behavior corresponds to curve (a) in Fig. 4.45.

$$\varepsilon_{fM} = \frac{6 f_M h}{L^2} \tag{4.141}$$

Flexural strain at break ε_{fB}: the normal flexural strain reached at specimen break.

$$\varepsilon_{fB} = \frac{6 f_B h}{L^2} \tag{4.142}$$

ISO 178 does not comply with these rules. Here, deflection is not represented by *f*, but by *s*. As stated in Section 4.3.5.1, the equations presented here are valid only for deflections that are relatively small compared to geometrical dimensions.

Corresponding to the standard, however, values as high as 6 mm for maximum possible deflection are distinctly higher. Thus under relatively large normal flexural strains and in the presence of inhomogeneities, off-center breaks can occur that corrupt the bend test result.

Figure 4.46 shows flexural stress–peripheral fiber strain diagrams of PP as a function of GF content. Flexural strength increases with fiber content, while tensile strain at break decreases. At the same time, it becomes clear that flexural strength can only be determined for high fiber contents (40 and 50 wt.-% in Fig. 4.46). In PP materials with low fiber content, flexural stress at conventional deflection is reached at 3.5 % peripheral fiber strain or 6 mm deflection, without a peak maximum or specimen

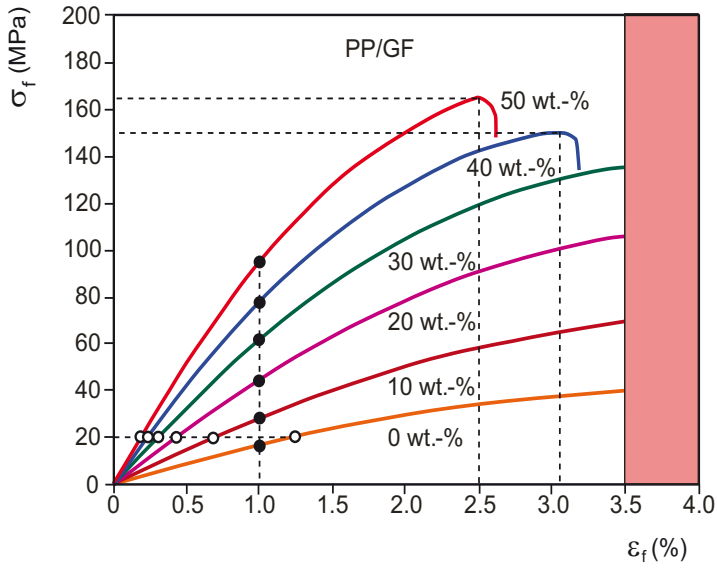

Fig. 4.46: Flexural stress–peripheral fiber strain diagrams of PP/GF composites as functions of GF content

break occurring. The flexural stress recorded for these materials at conventional deflection σ_{fC} is not comparable with flexural strength σ_{fM}. For this reason, the bend test mainly serves for quality control and the determination of material values for simple dimensioning tasks. The use of stress σ_x at x % of strain, which is not explicitly

Table 4.5: Selected characteristic values obtained from bend tests

Material	σ_{fM} (MPa)	σ_{fC} (MPa)	Material	σ_{fM} (MPa)	σ_{fC} (MPa)
Thermoplastics unreinforced			*Thermoplastics unreinforced*		
PE-HD		35	SAN	135	
PE-LD		10	PBT	85	70
PS	100		*Thermoplastics reinforced*		
PA 6		50	PP + 20 wt.-% GF		90
PC		70	PET+ 30 wt.-% GF	220	
PMMA	110		PBT+ 30 wt.-% GF	210	
PVC-U		100	*Thermosets*		
PVC-P		65	Phenole resin	70	
PP		35	Urea resin	70	
ABS		55	UP resin	60	
POM		120	PUR	110	

described in the standard, enables meaningful comparison of these materials. The expected tendency for strength to increase with increasing fiber content (● in Fig. 4.46) and the reduction in peripheral fiber strain (○ in Fig. 4.46) is reflected correctly with these parameters. Table 4.5 lists values from bend tests for selected plastics.

4.4 Impact Loading

4.4.1 Introduction

When products made from polymers are utilized in industrial practice, impact loading often occurs in addition to static loading. Examples of this include

- Demolding,
- Traffic accidents (crash),
- Underground assembly and laying of pipes,
- Hail impact on plastic rooves and window profiles,
- Stone impact on frontal surfaces of automotives and railroad rolling stock,
- Loading on plastic safety films and security glazing, and
- Accidents involving two-wheel vehicles (bicycle and motorcycle helmets).

Impact loading results in increased strain rate, significantly altering the strength and break behavior of most plastics. Besides increased strain rate, factors contributing to brittle fracture include low temperatures and multiaxial stress states including residual stresses. Stress concentrations at notches contribute especially to the formation of brittle fracture, so that tests are often performed on notched specimens.

The tests mostly used for evaluating the toughness of plastics under impact loading are the *Charpy* or notched *Charpy* impact test, the uniaxial impact or notched impact test, and the biaxial free-falling dart test owing to their relatively simple applicability. On specimens with rectangular cross-sections, plastic sheets and films, conventional toughness values are acquired that generally decrease with increasing strain rate, i.e., the occurrence of macroscopic brittle fracture phenomena is promoted.

The *Charpy* impact test in various arrangements has gained the greatest importance in the quality control of plastics because of its methodological simplicity, short testing time and relatively low consumption of materials. Although its use in quality assurance is undisputed, its applicability is limited in the area of material development and optimization (cf. Chapter 5).

When thermoplastics are tested, injection molded specimens are preferred because of their simple production technology (cf. Chapter 2). At the same time, internal states

- Adequate structural sensitivity or selectivity for the dominant damage mechanisms and
- Little or no influence from the sensors on the deformation behavior of the polymer.

Although many non-destructive test methods satisfy such requirements in principle, whenever possible, non-contacting and inertia-free sensoring techniques are to be preferred. In the following, various examples will be used to demonstrate the advantages and information potential of such hybrid test methods for polymer testing and polymer diagnostics [9.14, 9.15].

9.2 Tensile Test, Acoustic Emission Test and Video Thermography

By acoustic emission analysis or testing we mean a non-destructive acoustic test method used for characterizing initial damage in the deformation and fracture process, for observing damage kinetics and monitoring components. Generally speaking, crack formation and crack propagation processes, as well as phase transformations can be regarded as the causes of elastic stress waves or acoustic emissions (AE) occurring as a result of stress concentrations and subsequent exceeding of materials specific limit states.

Especially in filled and reinforced plastics, damage occurs particularly in the interfacial region between inclusions and matrix, where it acts as a sound source detectable by appropriate methods. A resonant or broadband transducer, a preamplifier and an acoustic emission analyzer are required to perform acoustic emission analysis (Fig. 9.2). In order to visually evaluate the resulting signal characteristic, it is advisable to couple the setup to a suitable oscilloscope. Depending on the type of loading and specimens used, the sensor should be attached with a suitable coupling agent (wax, oil) at sufficient distance to the active deformation region, while adequate receiver sensitivity has to be assured.

Thermographic test methods, such as the heat-flow method or vibro-thermography, are based on the fact that discontinuities or inhomogeneities in the material represent local changes in thermal conductivity. Reduced heat conduction in the range of developing or existing defects causes heat accumulation that, in turn, causes a temperature increase or thermal emission (TE). Due to the fact that most of the deformation work done is transformed into heat, in particular, energy dissipative damage mechanisms in matrix materials can be observed using this test method. For the relatively easy to realize procedure of video thermography, an infrared camera

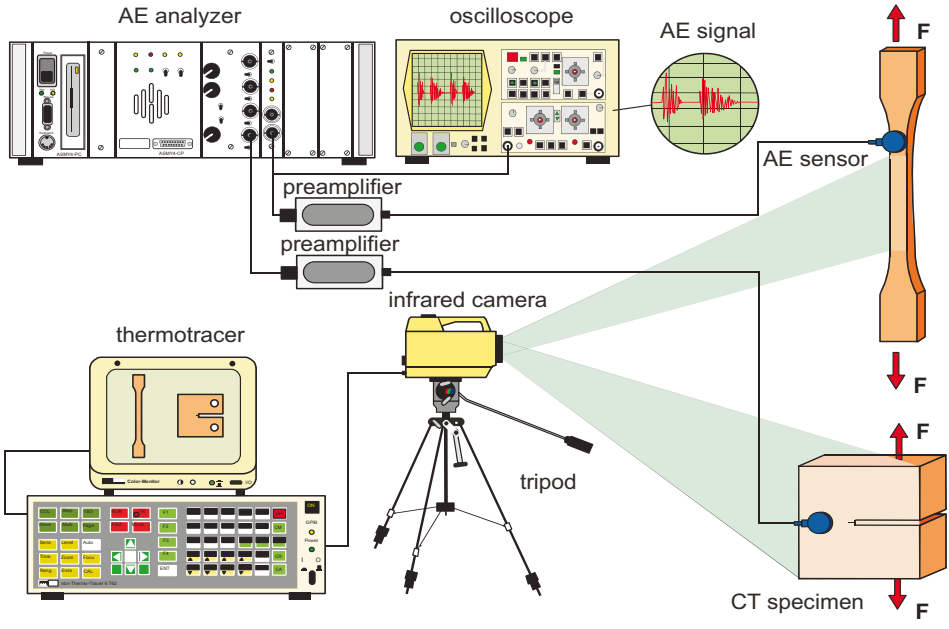

Fig. 9.2: Equipment for measuring acoustic emission and for video thermography on plastics materials

with sufficient time and temperature resolution, as well as a thermotracer (Fig. 9.2), are required for representing temperature fields or isotherms. The required reference temperature can be achieved by cooling the detector element with liquid nitrogen or by *Peltier* elements. To assure high temperature sensitivity and emissivity, the investigated specimen surface should be matt black, and the coating used must not cause any changes in the material behavior. In-depth information on both of these test methods, as well as more advanced measuring and evaluation technologies can be found, for instance, in [9.16] and [9.17].

Figure 9.3 shows an example for the simultaneous use of acoustic emission analysis and thermography for investigating mechanical damage behavior on polyamide 6 with 5 wt.-% short-glass-fiber in tensile tests. For the centrally notched multipurpose test specimens, a test speed of 5 mm min^{-1} was selected to assure high system resolution. The various measurement technologies can be synchronized via time or selected loading parameters (strain, stress). Although the continuous stress–strain curve (blue line) provides no information on the occurring damage processes, the registered acoustic emissions indicate active microdamage (red line). The disproportional increase in emissions and/or hits or events, termed onset ε_{AE} or critical strain, thereby indicates the beginning of irreversible damage in the interfacial region between fibers and matrix. The thermal diagram, as illustrated at the integral strain $\varepsilon_i = 1.8$ %, shows a surface cooling of approx. 4 °C compared to the original

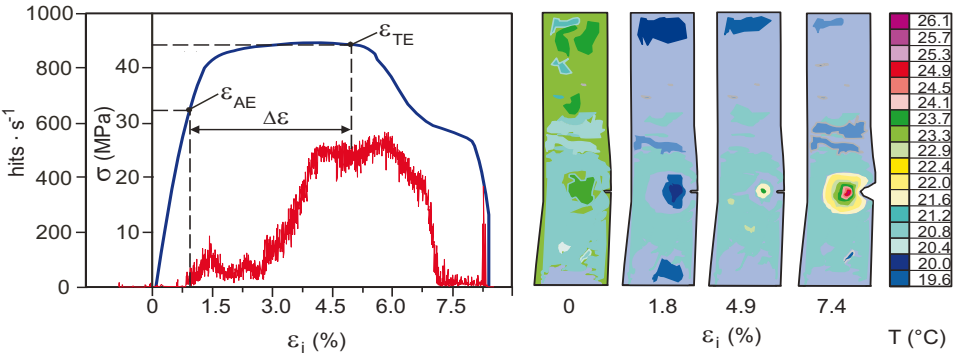

Fig. 9.3: Acoustic and thermal emissions from glass-fiber reinforced PA 6 in short-time tensile test

state due to the so-called thermoelastic effect. Simultaneously with the peak in acoustic activity, thermal onset ε_{TE} is observed to appear at 4.9 % strain. The drop in acoustic emissions starting at approx. 6.3 % is mainly due to crack edge friction in the interfacial region. The increasing warming is evidence of the dominance of plastic deformation in the polyamide matrix in the area surrounding the notch. From an engineering point of view, only the material behavior prior to beginning acoustic onset and the interval $\Delta\varepsilon$ are interesting, since mainly irreversible damage processes influencing strength take place in this deformation region of composite materials. Depending on loading and, in consequence, relaxation conditions, other functionalities are established specifically for various test temperatures and test speeds.

9.3 Tensile Test and Laser Extensometry

Laser Extensometry for Determining Local Deformation Behavior

Deformation and fracture behavior of plastics in the tensile test is measurably influenced by their processing-related internal state in addition to test-related conditions. Thus, structure and morphology parameters of the investigated specimen determine not only temporal and local deformation behavior, but also the amount and type of preliminary damage behavior. The deformation process in heterogeneous and anisotropic structured plastics is invariably accompanied by localization of external homogenenous deformation. A strain measuring technique with local resolution, such as laser extensometry, is thus required for understanding such processes. By laser extensometry, we generally mean scanning measuring techniques based on a transmission or reflexion principles that use the specimen as a beam barrier or reflector (Fig. 9.4) [9.11]. Deformation measurement with a maximum resolution of 0.1 µm involves registering time in relation to the scan velocity of a

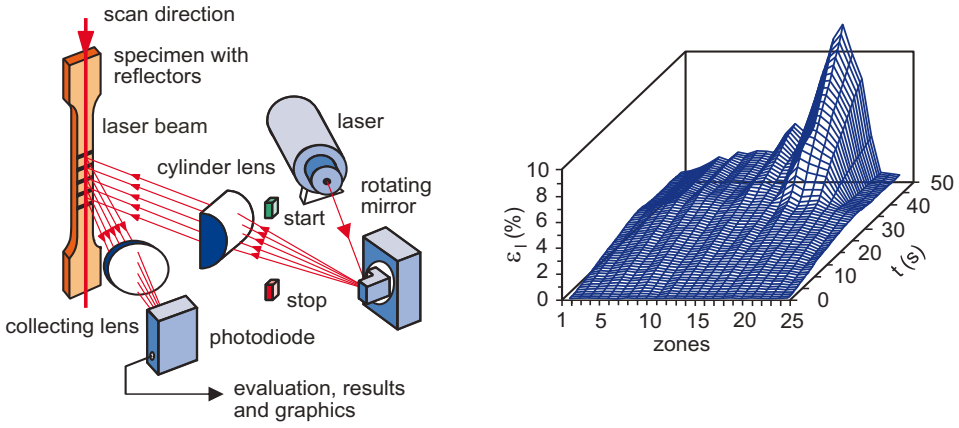

Fig. 9.4: Working principle of a laser extensometer (according to [9.18]) and local deformation distribution of ABS

rotating mirror or prism. In order to detect local strains, specimens have to be equipped with gauge marks or reflectors, usually at a minimum distance of 1 mm. The marks can be foil masks made by screen or tampon printing techniques, or they can be made by bright-dark contrasting with an air-brush or brush. Prior to the test start, approximately 20 scans are taken in the unloaded state to determine positioning of the reflectors, thus enabling the system to self-calibrate simultaneously. The fixed start and stop diodes serve to compensate variations in motor speed and to synchronize with the time signal of the universal testing machine. Laser beams reflected by the specimen are focused and processed by a junction diode for evaluation and presentation of results. From the registered local and integral strains, various graphic representations can be generated and values from the tensile tests calculated. The strain distribution presented in Fig. 9.4 for a specimen made from ABS with 26 reflectors is made up of 25 local strain–time diagrams over the length of the specimen. Up to the point where macroscopic necking forms, local strain is relatively homogeneously distributed, behaving inversely proportional to specimen orientation. The strong strain superelevation originating at approx. 35 s is caused by a local flow front, while strain constancy simultaneously appears in neighboring regions of the specimen. In addition to registering local deformation behavior, the high sensitivity of such measurement techniques enables detection of materials specific damage processes, especially for filled and reinforced polymers [9.19]. From the time dependence plotted in Fig. 9.5a for local strains ε_l in the investigated specimen region, the limit values of local strain ε_{lmax} and ε_{lmin}, as well as integral strain ε_i (Fig. 9.5b) and the corresponding stress–strain diagrams (Fig. 9.5c) can be determined, from which the tensile test values can be determined. As an additional characteristic parameter, heterogeneity (Fig. 9.5d) is included in the measurement range as the difference between maximum and minimum strain, in relation to integral

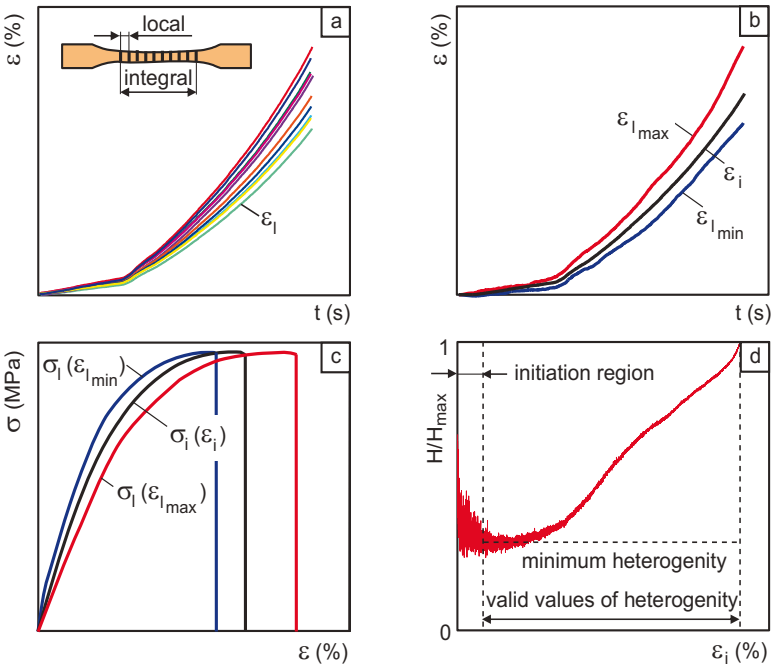

Fig. 9.5: Determining heterogeneity from local strain in the measurement interval: local strain behavior (a); local and integral strain–time functions (b); maximum, minimum and integral stress–strain diagrams (c) and normalized heterogeneity (d) as a function of integral strain

strain (Fig. 9.5c). The heterogeneity function (Fig. 9.5d) reflects influencing factors related to the material and its processing, as well as to testing technology. Knowledge of local independent maximum and minimum strain–time functions is required prior to making statements on heterogeneity, for which the following equation provides the computational basis (Eq. 9.1) [9.20]:

$$H(\varepsilon_i) = \frac{\varepsilon_{l\max} - \varepsilon_{l\min}}{\varepsilon_i} \tag{9.1}$$

When heterogeneity $H(\varepsilon_i)$ is normalized to the maximum occurring value $H(\varepsilon_i)/H_{max}$, a relative distribution between 0 and 1 is obtained (Fig. 9.5d) providing information on strain- or time-dependent materials changes.

The high heterogeneity at the start of the tensile test is obviously not due to structural processes, but to test-related influencing factors at low strains, and thus cannot be used for materials evaluation.

Figure 9.6 shows an application of laser extensometry involving the use of 32 reflectors for investigating the influence of coupling agents on the local deformation behavior of PA 66 with 30 wt.-% glass-fiber. From the strain distribution in Fig. 9.6

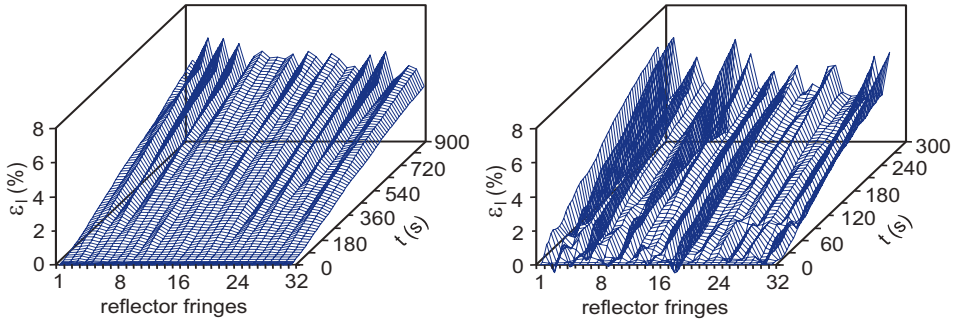

Fig. 9.6: Strain distribution for PA 66/30 wt.-% GF as a function of glass-fiber bonding [9.18]

(left), we can see that the strain occurring with efficient fiber–matrix coupling is relatively homogeneously distributed over the investigated measurement interval. By contrast, the strain distribution in Fig. 9.6 (right) exhibits heterogeneous behavior caused by the lack of a suitable coupling agent. This explains, why poor fiber–matrix coupling not only lowers the level of tensile strength, but also results in extremely uneven deformation behavior.

Because processing-related discontinuities affect polymer strain behavior in addition to such microstructural influencing factors, laser extensometry is also principally suited for investigating weld and joint lines (Fig. 9.7). When 4 mm thick PA 6 plates with 10 and 30 wt.-% short-glass-fibers are joint by heated-tool welding, an approx. 1 mm wide weld line results, as shown by the sketch in Fig. 9.7 [9.21, 9.22]. When specimens prepared from the welded plates are investigated using laser extensometry, an approx. 10 mm wide zone of welding influence can be detected, exhibiting

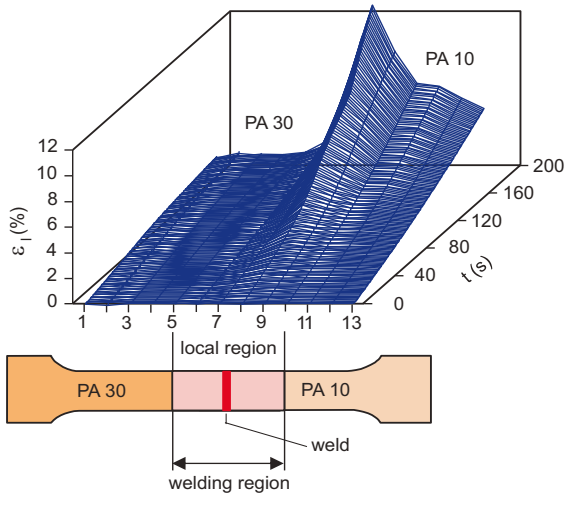

Fig. 9.7: Influence of weld lines on local deformation behavior of glass-fiber reinforced polyamides [(PA 10 (PA 6/10 wt.-% GF); PA 30 (PA 6/30 wt.-% GF)]

pronounced strain superelevation due to altered orientation. By contrast, the regions not influenced by the welding process exhibit a deformation behavior corresponding to the various glass-fiber contents of the original plates. Based on these results, in order to evaluate weld quality, it is not sufficient to state a welding coefficient as the ratio between weld strength and base materials strength, especially since that method is not applicable where different materials are welded.

Laser Multiscanner for Detecting Local Deformation Fields

When specimen geometries diverge from those of standard specimens in the tensile test, it should be practice to simulate the influence of various widths or predetermined breaking points on plastics deformation behavior. Since with increasing width, deformation disability appears in transverse strain (transition from a plane-stress to a plane-strain state), stresses arise simultaneously in the transverse direction, and local deformation over the specimen width is nonuniform. A laser multiscanner can be used for such experimental investigations (Fig. 9.8), which provides results on local strain as a function of width in addition to local longitudinal strain.

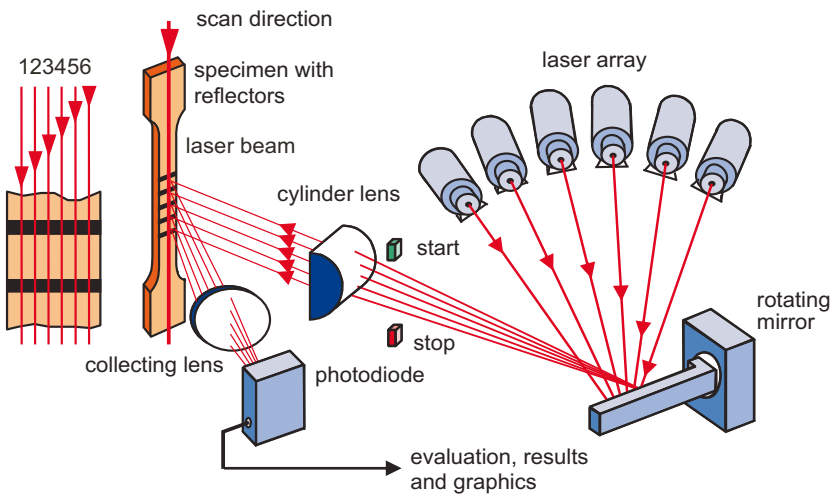

Fig. 9.8: Schematic setup of a laser multiscanner

Like the laser extensometer, a multiscanner works on the basic principle of local strain measurement, but uses a laser field consisting of 6 different semiconductor laser diodes. Laser beams adjustable over a range of up to 50 mm scan the specimen with slight time shifts at various positions. The measuring system illustrated is also self-calibrating and achieves a resolution of approx. 1 µm at a scan rate of 40 ms and a working distance of 200 mm. An example is the investigation of local deformation

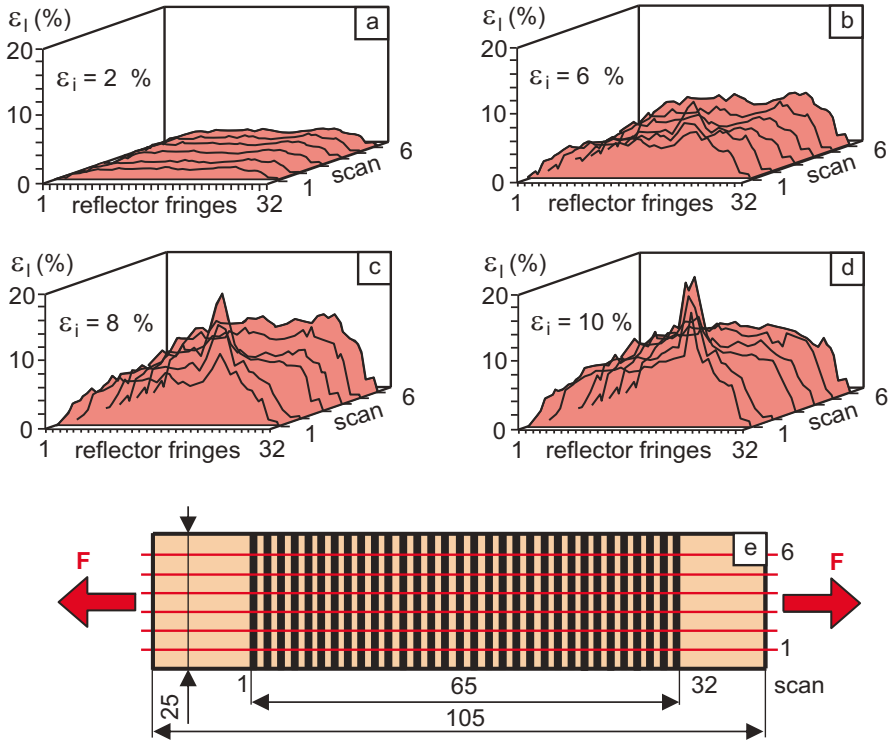

Fig. 9.9: Use of a laser multiscanner for investigating polymer films

behavior in a polyester film (Fig. 9.9). Within the 65 mm measuring window, the 0.35 mm thick film contains 32 reflectors spaced 1 mm apart. In the tensile test performed at 10 mm min^{-1}, strain superelevation can be clearly observed in the area of laser beams 1 and 2 at an integral strain as low as 6 % (Fig. 9.9b). This local deformation peak is caused by a film thickness difference of 0.1 mm, given a standard thickness of 0.35 mm. Simultaneously with the flow processes induced in the area of these defects, relaxations occur in other regions of the polyester film that can be detected by the sensitive laser multiscanner. [9.23] and [9.24] list further application examples of laser extensometers for high-temperature and high-speed polymer testing ranges.

9.4 Fracture Mechanics and Non-Destructive Testing

Bend Test and Microscopy

In-situ crack tip monitoring is required during the loading procedure in the fracture mechanics experiment if we wish to include physical crack initiation when describing the deformation and fracture behavior of polymer materials with fracture mechanical